Journal of Quantitative Spectroscopy & Radiative Transfer 347 (2025) 109654

Contents lists available at ScienceDirect

Journal of Quantitative Spectroscopy and Radiative Transfer

journal homepage: www.elsevier.com/locate/jqsrt

The vacuum ultraviolet photoabsorption spectroscopy of 1-Bromo-2,2-Difluoroethylene ($BrHC{=}CF_2$). A joint experimental and quantum chemical investigation

R. Locht [a,*], C. Kune [b]

[a] MolSys Research Unit, Molecular Dynamics Laboratory, Department of Chemistry, Institute of Chemistry, BldgB6c, University of Liège, Sart-Tilman, B-4000 Liège 1, Belgium

[b] MolSys Research Unit, Mass Spectrometry Laboratory, Department of Chemistry, Institute of Chemistry, Bldg B6c, University of Liège, Sart-Tilman, B-4000 Liège1, Belgium

ARTICLE INFO

Keywords:
Vacuum UV photoabsorption Synchrotron Radiation Quantum chemical calculations Valence and Rydberg states Electronic and vibrational transitions 1-bromo-2,2-difluoroethylene

ABSTRACT

The vacuum UV photoabsorption spectrum of 1-bromo-2,2-difluoro-ethylene has been observed using synchrotron radiation. It is measured and analyzed between 5 eV (40300 cm^{-1}) and 15 eV (121000 cm^{-1}) for the first time. Several very weak features are observed at low photon energy, between 5.0 eV and 6.5 eV, and assigned to valence transitions. To support the assignment of these features, quantum chemical calculations have been performed on the excitation energies of the neutral states of $BrHC{=}CF_2$. The characteristic $\pi_{CC}(4a'')\rightarrow\pi_{CC}^*(a'')$ valence transition for the ethylene derivatives is observed at 6.955 eV. The detected vibrational structure is assigned to ν_2 (C=C stretching) and ν_6 (C-Br stretching) vibrations with vibrational wavenumbers ω_2=1550±60 cm^{-1} (192±7 meV) and ω_6=790±60 cm^{-1} (98±7 meV). Between 7.4 eV and 9.8 eV numerous weak but sharp transitions are observed, classified and assigned to $\pi_{CC}(4a'')\rightarrow np\lambda$ (n=5-10, λ=0,1) and nd (n=4-7) Rydberg transitions converging to $IE_{ad}(\tilde{X}^2A'')$=9.695 eV [5]. Their vibrational structure has been analyzed and assigned to ν_2 (C=C stretching), ν_6 (C-Br stretching) and ν_8 (CF_2 rocking) vibrational normal modes. Averaging over all the npλ and nd Rydberg states, the vibrational wavenumbers $\overline{\omega}_2$= 1520±20 cm^{-1} (188±3 meV), $\overline{\omega}_6$=770±20 cm^{-1} (95±3 meV) and $\overline{\omega}_8$=363±20 cm^{-1} (45±3 meV) are obtained. The 9.2 eV to 11.0 eV region is dominated by strong and sharp Rydberg transitions converging to $IE_{ad}(\tilde{A}^2A')$=11.362 eV [5]. Transitions from $n_{Br}(11a')\rightarrow ns$ (n=5-9), np (n=5-9) and ndλ (n=4-9, λ=0,1) are observed. Their analysis shows the excitation of ν_4 (C-F symmetric stretching) and ν_8 (CF_2 rocking) vibrational normal modes. These are characterized by averaged vibrational wavenumbers$\overline{\omega}_4$=1125±40 cm^{-1} (139±5 meV) and $\overline{\omega}_8$=366±40 cm^{-1} (45±5 meV). Above 11.0 eV and up to 15.0 eV sharp strong absorption is followed by long series of weak modulations superimposed on strong broad bands. An analysis and interpretations of these features have been attempted in terms of Rydberg transitions converging to the successive vertical ionization energies at 12.59 eV, 14.48 eV, 15.62 eV and 16.14 eV [5]. In the former case a long vibrational progression is assigned to $\overline{\omega}_7$=508±20 cm^{-1} (63±3 meV) combined with $\overline{\omega}_9$=130±16 cm^{-1} (16±2 meV). In the three latter cases, the weak modulations have mainly been assigned to ν_8 (CF_2 rocking) vibrations with $\overline{\omega}_8$=325±30 cm^{-1} (45±4 meV).

1. Introduction

To the best of our knowledge very scarce are the investigations devoted to the title molecule. Very few or even non-existent are the data related to its physical and chemical properties.

Theimer and Nielsen [1] reported about the infrared and Raman spectroscopy of the $BrHC{=}CF_2$ molecule. The twelve fundamental vibrational wavenumbers were observed, measured and assigned.

More recently Orkin et al. [2] investigated the reactivity of $BrHC{=}CF_2$ with OH radicals. They measured the absolute photoabsorption cross section of $BrHC{=}CF_2$ in the ultraviolet region between 164 nm and 266 nm (7.56-4.66 eV). No interpretation or assignment has been reported. The atmospheric implications of this compound as ODP (Ozone Depleting Potentials) are mainly considered and discussed.

* Corresponding author.
E-mail address: robert.locht@uliege.be (R. Locht).

https://doi.org/10.1016/j.jqsrt.2025.109654
Received 31 July 2025; Received in revised form 27 August 2025; Accepted 2 September 2025
Available online 3 September 2025

We recently reported on the ionization and the vacuum ultraviolet photoabsorption spectroscopy (PAS) of 1,1-dibromoethylene ($Br_2C{=}CH_2$) [3] and 1,1-dibromo-2,2-difluoroethylene ($Br_2C{=}CF_2$) [4]. Detailed analyses and assignments were proposed. The aim of the present work is the investigation of the photo-induced processes of absorption, ionization and dissociation of 1-bromo-2,2-difluoroethylene ($BrHC{=}CF_2$) in the vacuum ultraviolet (VUV) between 5 eV (248 nm or 40 300 cm^{-1}) and 15 eV (83 nm or 121 000 cm^{-1}). As a first part, the photoabsorption spectroscopy (PAS) of $BrHC{=}CF_2$ will be presented and discussed in detail in the present paper. The photoionization and photodissociation processes observed in this molecule will be described and discussed in a forthcoming publication [5].

2. Experimental

2.1. Experimental setup

The experimental setup used in the present work has been described in detail previously [6]. Only the most important features will be addressed here.

The 3m-NIM monochromator at the 3m-NIM2 beam line at BESSY II (Berlin, Germany) is equipped with an Al/MgF_2 600 lines/mm spherical grating. The spectra discussed in the present work were measured with 40 μm entrance and 5 μm exit slits. Light is detected by a sodium salicylate sensitized photomultiplier located at the end of a windowless stainless steel 30 cm long absorption cell. A differential pressure ratio of 1:1 000 is maintained with a 1 mm thick stainless steel microchannel plate inserted between the exit slit of the monochromator and the entrance of the absorption cell. A Balzers capacitor manometer is used to measure the vapor pressure in the cell. The output pulses from the photomultiplier are recorded by a 100 MHz counter. The recording of an absorption spectrum requires one scan with gas in the absorption cell and one with the evacuated cell.

The 1-bromo-2,2-difluoro-ethylene ($BrHC_2F_2$) available from ABCR at 98% purity, checked by mass spectrometry, was used without further purification.

2.2. Data treatment and Uncertainty estimation

In the photoabsorption spectrum (PAS) a strong continuum often underlies weak sharp peaks and diffuse structures. A continuum subtraction procedure is applied to characterize more easily and accurately these features. It is consisting of a severe smoothing of the experimental curve by fast Fourier transform (FFT) to simulate the underlying continuum. The result is subtracted from the original PAS. Weak features emerge from a strongly attenuated background. This procedure has been thoroughly investigated and validated by Marmet and Carbonneau [7–10]. In the forthcoming sections the resulting diagram is called Δ-plot. This method has already successfully been used in previous spectral analyses [11,12].

The multiple lines vacuum UV-PAS of N_2 [13] has been used to calibrate the monochromator. The accuracy of this calibration is better than 2 meV. The measurements have been repeated several times. The PAS between 5 eV and 15 eV has been recorded with energy increments of 10 meV. In most other series of measurements an increment of 1.0 meV is maintained between 6 eV and 14 eV. An energy increment of 0.2 meV has been adopted for the recording of the 11.0-11.4 eV range. The error on the energy position of a feature is estimated to be 2 meV including the calibration error.

3. Experimental results

An overview of the vacuum UV-PAS of $BrHC_2F_2$ recorded between 5 eV and 15 eV photon energy range is shown in Fig. 1. Valence and Rydberg transitions are indicated by vertical bars. The successive adiabatic and/or vertical ionization energies (dashed lines), as determined by HeI-photoelectron spectroscopy (PES) [5] and used as convergence limits of the Rydberg series, are inserted.

This PAS consists of a succession of many weak and a few strong sharp lines. It could be clearly divided into four quite different regions: (i) a region of a few very weak to weak broad bands between 5.0 eV and 7.4 eV, (ii) numerous weak but sharp lines superimposed on a weak continuum between 7.4 eV and 10.4 eV, (iii) many weak to strong sharp lines superimposed on a continuum steeply rising from 10.4 eV to 11.6 eV and (iv) five broad strong bands spreading between 11.4 eV and 15.0 eV. In addition, a very weak dense structure is observed in the region extending from 11.0 eV to 12.5 eV photon energy range.

The energy position of the vibrationless Rydberg transitions converging to the first two adiabatic convergence limits are listed in Table 1. Assignments and characteristics, i.e. average quantum defects $\bar{\delta}$and individual effective quantum numbers n*, are included.

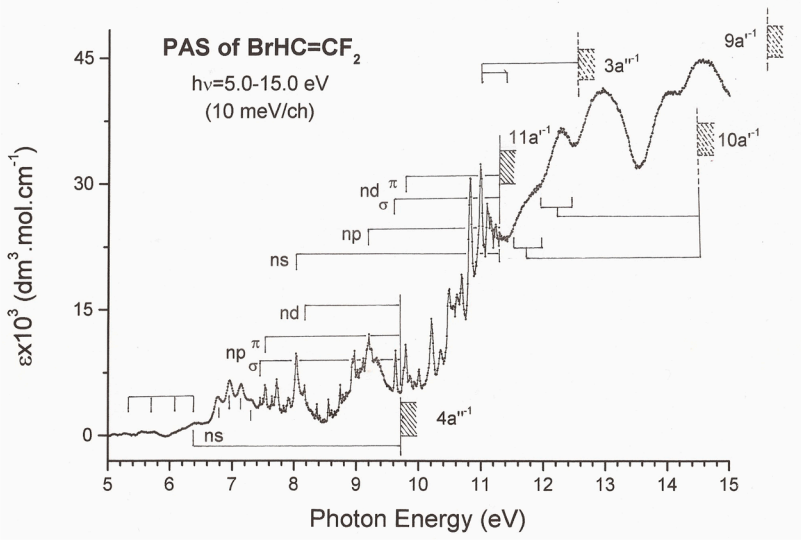

Fig. 1. Vacuum UV-PAS of $BrHC_2F_2$ between 5 eV and 15 eV photon energy using synchrotron radiation (10 meV increments). Small vertical bars and shaded areas locate members of Rydberg series and their respective convergence limits [5]. Dashed areas indicate vertical ionization energies. Square brackets indicate vibrational progressions of Rydberg states converging to IE_{vert}=14.48 eV [5].

Table 1
Rydberg series observed in the vacuum UV photoabsorption spectrum of $BrHC_2F_2$ converging to the first two adiabatic ionization energies (IE_{ad}). Excitation energies (eV), wavenumbers (cm^{-1}), effective quantum numbers (n*) and average quantum defects ($\bar{\delta}$) measured in the present work. Conversion factor: 1 eV= 8065.545 eV [21,22].

eV Rydb.Ser. to IE_{ad}=9.695 eV[a]	cm^{-1}	n*
4a"→npσ ($\bar{\delta}$=2.54±0.03)		
7.450	60088	2.462
8.557	69017	3.458
9.004	72622	4.437
9.238	74510	5.456
9.364	75526	6.411
9.454	76252	7.514
4a"→npπ ($\bar{\delta}$=2.48±0.05)		
7.532	60750	2.508
8.598	69348	3.522
9.016	72719	4.476
9.246	74574	5.505
9.373	75598	6.500
9.461	76308	7.625
4a"→nd ($\bar{\delta}$=1.00±0.02)		
8.173	65620	2.990
8.837	71275	3.982
9.151	73808	5.001
9.320	75171	6.023
Rydb.Ser. to IE_{ad}=11.362 eV[a]		
11a'→ns ($\bar{\delta}$=2.97±0.03)		
8.033	64790	2.019
9.874	79639	3.016
10.526	84898	4.015
10.826	87317	5.038
10.994	88673	6.080
11a'→np ($\bar{\delta}$=2.49±0.06)		
9.200	74203	2.504
10.203	82293	3.428
10.687	86196	4.463
10.924	88108	5.576
11.037	89019	6.470
11a'→ndσ ($\bar{\delta}$=1.16±0.04)		
9.631	77679	2.804
10.459	84358	3.885
10.791	87035	4.881
10.966	88447	5.861
11.070	89286	6.826
11.137	89826	7.776
11a'→ndπ ($\bar{\delta}$=1.07±0.05)		
9.795	79002	2.939
10.473	84470	3.895
10.805	87148	4.907
10.979	88552	5.899
11.086	89415	7.021

[a] Adiabatic ionization energies measured by HeI-PES [5].

4. *Ab initio* calculations

The molecular orbital configuration of $BrHC_2F_2$ in the C_S symmetry point group is described by:

$1s^2$(Br) $2s^2$(Br) $2p^6_{x,y,z}$(Br) $1s^2$(F1) $1s^2$(F2) $1s^2$(C1) $1s^2$(C2) $3s^2$(Br) $3p^6_{x,y,z}$(Br) $3d^{10}$(Br) $1a'^2$ $2a'^2$ $3a'^2$ $4a'^2$ $5a'^2$ $6a'^2$ $1a''^2$ $7a'^2$ $8a'^2$ $2a''^2$ $9a'^2$ $10a'^2$ $3a''^2$ $11a'^2$ $4a''^2$: $\tilde{X}^1A'$ where the 1a' orbital is the first outer-valence shell orbital and the 4a"orbital is the highest occupied orbital (HOMO) represented in Fig. 2a. The lowest unoccupied molecular orbital (LUMO) is the 12a' orbital and shown in Fig. 2b.

4.1. Computational tools

The calculations presented in the present work have been performed using the Gaussian 09 revision D.01 program [14].

The geometry optimization in the C_S symmetry point group was performed at DFT [16] and TDDFT [17] levels using both M06-2X [18] and B3LYP [19,20] as pseudopotential. The 6-311G++(d,p) [15] basis set has been used for all calculations. This basis set has preferentially been used as providing a good compromise between accuracy and computational cost. The obtained results are in good agreement with the available experimental data [1], while requiring significantly lower computational resources compared to more extended basis sets such as the cc-pVnZ series. The vertical excitation energies from the ground state to several neutral excited states (and their associated oscillator strength) have been calculated. The results obtained at the B3LYP-level are listed in Table S1 of the Supplementary Material section.

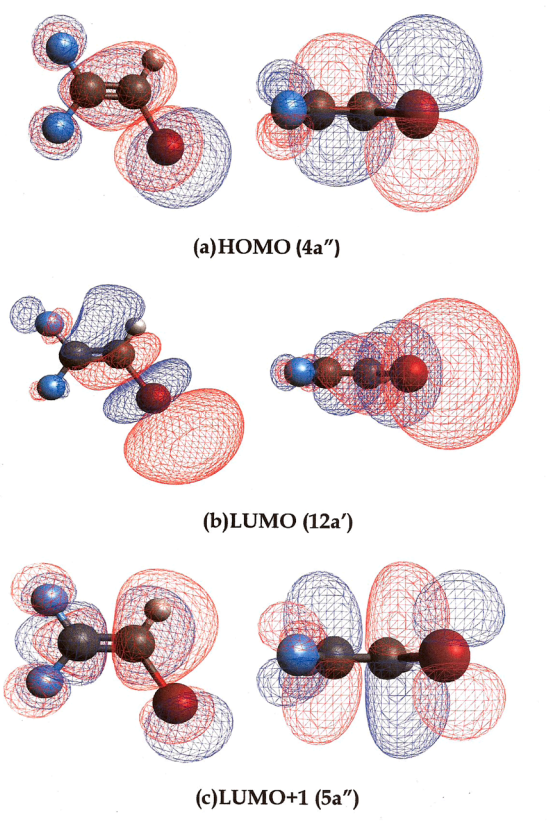

Fig. 2. In $BrHC_2F_2$ shape of (a) the highest occupied molecular orbital (HOMO) 4a", (b) the lowest unoccupied molecular orbital (LUMO) 12a' and (c) the LUMO+ 1 (5a") molecular orbital at the DFT/B3LYP level. Contours correspond to an isovalue of 0.02. The positive and negative parts are colored in blue and red respectively.

4.2. The Calculation results for the lowest neutral states

The optimized geometry parameters of the eight lowest-lying neutral states have been calculated at the M06-2X and B3LYP levels and are listed in Table S2 (see Supplementary Material). The results are in quite good agreement for both calculation levels. However, noteworthy is the discrepancy for the 3^1A" state: all internuclear distances are larger in the B3LYP than by the M06-2X calculation.

The vertical excitation energy and the oscillator strength for the lowest neutral excited states, of interest in the present work, were calculated at both M02-6X and B3LYP levels. The results for the seven first neutral states are listed in Table 2a.

The transition energies are systematically lower for the B3LYP calculations. The 1^1A" and 2^1A" states, characterized by nearly identical geometry, are separated by about 1.0 eV. These states being of same symmetry, should likely strongly couple. The presence of imaginary wavenumbers (see Table 2c) has probably to be ascribed to this interaction. The first two transitions should correspond to $\pi_{CC}\rightarrow\sigma_{CBr}^*/\sigma_{CH}^*$

Table 2
(a) Vertical excitation energy (E_{vert}) and oscillator strength (OS) associated with the lowest excited neutral states of BrHC=CF_2 calculated at the M06-2X and B3LYP levels. (b) Calculated vibrational wavenumbers (cm^{-1}) of the neutral ground state and the $3^1A'$ excited state of BrHC=CF_2. Comparison between theory and experiment [1] is made for the $\tilde{X}^1A'$ground state. (c) Vibrational wavenumbers (cm^{-1}) of the first neutral excited states calculated at the B3LYP level.

(a)

	M06-2X/ 6-311G++(d,p)		B3LYP/ 6-311G++(d,p)	
States	E_{vert} (eV)	OS (f)	E_{vert} (eV)	OS (f)
$1^1A"$	5.307	0.0004	5.139	0.0008
$2^1A"$	6.421	0.0002	6.157	0.0008
$2^1A'$	6.450	0.0010	6.327	0.0020
$3^1A'$	7.094	0.2740	6.743	0.2300
$3^1A"$	7.304	0.0000	6.950	0.0000
$4^1A"$	7.623	0.0030	7.058	0.0000
$5^1A"$	7.653	0.0500	7.380	0.0440

(b)

States	$\tilde{X}^1A'$			$3^1A'$	
Modes	Exp [1]	M06-2X	B3LYP	M06-2X	B3LYP
a'					
ν_1	3135	3268	3250	2802	2598
ν_2	1736	1820	1768	1629	1559
ν_3	1317	1366	1311	1490	1391
ν_4	1172	1206	1175	1235	1185
ν_5	959	991	958	1005	940
ν_6	767	791	764	851	808
ν_7	568	580	566	581	662
ν_8	369	380	368	393	544
ν_9	164	171	168	182	337
a"					
ν_{10}	741	779	764	2393	1804
ν_{11}	583	629	600	670	185
ν_{12}	227	213	211	160	175

(c)

States	$\tilde{X}^1A'$		$1^1A"$	$2^1A"$	$2^1A'$		$3^1A'$	$3^1A"$		$4^1A"$	$5^1A"$
Modes	Exp [1]	B3LYP									
a'											
ν_1	3135	3250	3234	3226	3624		2598	2584		3175	2750
ν_2	1736	1768	1493	1612	1293		1559	1517		1706	1780
ν_3	1317	1311	1206	1257	1158		1391	1261		1564	1262
ν_4	1172	1175	936	947	990		1185	1117		1186	1132
ν_5	959	958	748	912	818		940	925		1070	839
ν_6	767	765	565	554	633		808	665		690	639
ν_7	568	566	491	520	463		662	486		503	507
ν_8	369	368	210	237	339		544	333		**323**	356
ν_9	164	168	77	24	257		377	127		***i109****	126
a"											
ν_{10}	741	764	807	626	3207	1804		3360	981		1262
ν_{11}	583	600	601	598	523	185		***i727****	***i540****		575
ν_{12}	227	211	***i13****	9	188	175		***i1068****	***i1332****		205

* Imaginary wavenumbers are in italic type.

($1^1A"$) and $\pi_{CC} \rightarrow Rs_{Br}$ ($2^1A"$) compatible with the large C-Br elongation. However, these transitions should not be allowed and are characterized by nearly zero oscillator strength.

The excitation to the $2^1A'$ state is the first allowed transition. It is lying at about 6.4 eV above the ground state. Despite the symmetry of the final state, the transition has small oscillator strength. This state shows a very large elongated C=C bondlength (+0.14 Å) and strongly modified wavenumbers ν_2 (-475 cm^{-1}) and ν_{10} (+2442 cm^{-1}) at the B3LYP level (see Table 2c). As shown in Table S3, the same result is obtained at M06-2X level, but where additionally the ν_{12} wavenumber becomes imaginary (*i*850 cm^{-1}) likely indicating the occurrence of a transition state.

The most probable transition in the low-energy range has to be assigned to the transition to the 5a"(π^*_{CC}) orbital giving rise to the $3^1A'$ state and represented in Fig. 2c. The obtained final state shows a C=C bond elongation (+0.0648 **Å**) and the C-Br and both C-F bonds shortening (-0.0861, -0.0335 and -0.0410 **Å**). Both the H-C-Br and F-C-F angles are significantly opened.

The predicted vibrational wavenumbers calculated at both levels could only be compared with the existing experimental results for the neutral ground state listed in Table 2b. Obviously, the best agreement is observed at the B3LYP level. Table 2c displays the predicted wavenumbers obtained at this level for the first seven excited states. The $1^1A"$ appears to be likely a transition state with an imaginary ν_{12}=*i*13 cm^{-1}. The $3^1A"$and $4^1A"$ states are second (CP2) and third (CP3) order critical point states with two and three imaginary wavenumbers. The transition to these states show zero or nearly zero oscillator strength. The corresponding results obtained at the M06-2X level are displayed in Table S3 (see Supplementary Material), generating $2^1A"$ and $2^1A'$ states as transition states (TS).

5. Discussion

The vacuum UV-PAS is essentially made of valence and Rydberg

transitions. The former are usually broad and diffuse whereas the latter are numerous and sharp. Providing no Rydberg-Rydberg interaction is considered, the sharp bands appearing in the spectrum can be assigned according to the Rydberg formula:

$$E_{Ryab} = IE - R/(n-\delta)^2 = IE - R/n^{*2} \quad (1)$$

where R is the Rydberg constant R=13.606 eV [21,22], δ is the quantum defect, n* is the effective quantum number and IE is the ionization energy or the convergence limit of the considered Rydberg series. The successive ionization energies IE to be used will be defined elsewhere [5] and are inserted in Fig. 1. Adiabatic ionization energies (IE_{ad}) are used for members of series involving a well defined vibrationless transition. Otherwise, the vertical ionization energy (IE_{vert}) has been adopted. The term R/n^{*2} is called the term value T characterizing the considered Rydberg series. Trend values of T, and implicitly of n* and δ, for ns-, np- and nd-type Rydberg series are observed and have been thoroughly investigated and discussed [23]. On this basis the Rydberg transitions observed between 7.4 eV and 11.1 eV in the vacuum UV-PAS of $BrHC_2F_2$ have been classified and are listed in Table 1.

5.1. Valence Transitions between 5.0 eV and 7.4 eV (see Figs. 1 and 3)

As shown in Fig.1 this energy range is dominated by a weak well structured but broad band peaking at 6.955 eV. It is superimposed on a very weak continuum made of at least four broad peaks showing a maximum at about 5.53 eV, 5.74 eV, 6.12 eV and 6.40 eV (see Fig.1 and Fig. 3) and listed in Table 3.

The weakest and lowest energetic continuum shows at least maxima at 5.53 eV and 5.74 eV. Using the present calculation results, only the $1^1A''$ state is obtained at 5.139 eV and corresponding to a $\pi_{CC}\rightarrow\sigma_{CBr}^*$/$\sigma_{CH}^*$ excitation. This forbidden transition should be very weak. The energy separation of about 0.21 eV (1690 cm^{-1}) could tentatively be assigned to the ν_2 vibrational excitation calculated at 1493 cm^{-1}.

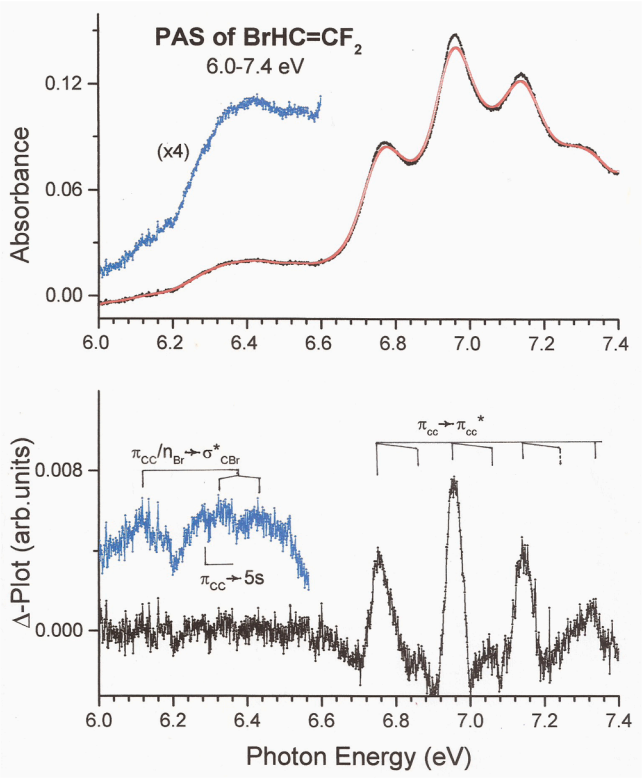

Fig. 3. Vacuum UV-PAS of $BrHC_2F_2$ between 6.0 eV and 7.4 eV photon energy (1.0 meV increments). The upper panel shows the absorbance (black curve). The red curve corresponds to the FFT smoothing. The lower panel shows the corresponding Δ-plot. Vertical bars locate critical energies and the proposed vibrational structure.

Table 3
Vertical (E_{vert}) excitation energies (eV) and oscillator strength (f) calculated and observed in the vacuum UV photoabsorption spectrum of $BrHC_2F_2$ and corresponding to (a) the broad weak absorption bands between 5.0 eV and 7.0 eV and (b) the vibrational structure in the valence $\pi_{CC}\rightarrow\pi_{CC}^*$ ($3^1A'$) excited state and its assignment. Conversion factor: 1 eV= 8065.545 eV [21,22].

a)

Theory: E_{vert}/f				Expt.	Description
M06-2X		B3LYP			
E_{vert} (eV)	f	E_{vert} (eV)	f	E_{vert} (eV)	
5.307	0.0004			5.53	$\pi_{cc}\rightarrow\sigma_{CBr}^*/\sigma_{CH}^*$: $1^1A''$
		5.139	0.0008		
				5.74	
6.421	0.0002	6.157	0.0008	6.12	$\pi_{cc}\rightarrow\sigma_{CBr}^*$: $2^1A''$
6.450	0.0010	6.327	0.0020	6.39	$n_{Br}\rightarrow\sigma_{CBr}^*/\sigma_{CH}^*$: $2^1A'$ [4a"(π) - Rs]
7.094	0.2740	6.743	0.2300	6.955	4a"(π)→π*: $3^1A'$

(b)

$3^1A'$

E_{exc} (eV)	E_{exc} (cm^{-1})	Assignment	
6.756	54491	**(0,0)**	ω_2=192±7 meV
6.861	55338	ν_6	1550±60 cm^{-1}
6.955	56096	$\boldsymbol{\nu_2}$	ω_6=98±7 meV
7.046	56830	$\nu_2+\nu_6$	790±60 cm^{-1}
7.140	57588	$\mathbf{2\nu_2}$	
7.238	58378	$2\nu_2+\nu_6$	
7.332	59137	$\mathbf{3\nu_2}$	

Resulting from the present calculations, the continuum measured at 6.12 eV in the Δ-plot of this region would involve the $n_{Br}\rightarrow Rs$ ($2^1A''$) transition calculated at 6.157 eV. This transition is also forbidden and is corresponding to a weak band in the observed spectrum.

A second stronger but very broad continuum is spreading from 6.2 eV-6.6 eV and centered at about 6.40 eV. Despite the unfavorable signal/noise ratio, the Δ-plot of this region would show four submaxima at 6.28 eV, 6.34 eV, 6.40 eV and 6.47 eV respectively (see Fig.3, lower panel). By quantum chemical calculations, a $2^1A'$ state is obtained at 6.327 eV excitation energy corresponding to a $n_{Br}\rightarrow\sigma_{CBr}^*$/$\pi_{CC}$ transition. A similar n_{Br}-lone pair MO excitation was calculated at about 6.1 eV in the vacuum UV-PAS of $Br_2C{=}CF_2$ [4].

The signal at 6.28 eV could also very likely correspond to the lowest π_{CC}(4a")→5 s Rydberg transition. Using $IE_{ad}(\tilde{X}^2A'')$=9.695 eV [5], the evaluated term value T= 3.41 eV leads to an effective quantum number n*=2.00 and a quantum defect δ=3.00. A corresponding transition was observed at 6.18 eV and 6.585 eV in the vacuum UV-PAS of $Br_2C{=}CF_2$ [4] and $H_2C{=}CBr_2$ [3] respectively. The set of features observed between 6.28 eV and 6.47 eV could likely be assigned to a vibrational progression pertaining to the same transition. The large width of the signals could be related to the lifetime of the individual vibrational levels.

The major band with vertical excitation energy E_{vert}=6.955 eV has been assigned to the π_{CC}(4a")→π_{CC}^*(5a") valence transition to the $3^1A'$ state. By quantum chemical calculation the corresponding vertical transition energy is predicted at 7.094 eV or 6.743 eV at M06-2X or B3LYP level respectively. The corresponding vertical excitation was observed at 6.231 eV, 7.482 eV and 6.920 eV in the vacuum UV-PAS of the related molecules $Br_2C{=}CH_2$ [3], $H_2C{=}CF_2$ [24] and $Br_2C{=}CF_2$ [4] respectively.

The vibrational structure of this band has been analyzed in terms of a short progression involving ν_2 (C=C stretching) and ν_6 (C-Br stretching) vibrations as listed in Table 3b. The vibrational wavenumbers ω_2=1550 ±60 cm^{-1} (192±7 meV) and ω_6=790±60 cm^{-1} (98±7 meV) have been

measured. Quantum chemical calculations provided 1559 cm^{-1} and 808 cm^{-1}. These values could be compared to those observed for the ground state of the neutral molecule where ω_2=1736 cm^{-1} and ω_6=767 cm^{-1} successively [1]. The ν_2 vibrational mode is expected to be mostly affected, the π(C=C) highest occupied 4a" MO (HOMO) being mainly involved in this transition.

5.2. Rydberg Transitions

5.2.1. ***Rydberg series converging to $IE_{ad}(\tilde{X}^2A")$=9.695 eV*** *[5] (see Fig. 4)*

The vacuum UV-PAS measured between 7.4 eV and 9.8 eV is displayed in Fig. 4 together with the corresponding Δ-plot. Disentangling the numerous features observed in this energy range, the Franck-Condon profile of the first HeI-PES band [5] has been used as a guide as illustrated in Fig. 4 (a-c). The energy positions, the Rydberg transition types and vibrational progressions are listed in Table 4.

The considered energy range is clearly dominated by 4a"→npλ and nd Rydberg transitions. Both the 4a"→npσ (Fig. 4a) and 4a"→npπ (Fig. 4b) transitions are observed for n=5-10. By quantum chemical calculations transitions to the 5pσ and 4d states have been located at 7.380 eV and 8.287 eV respectively whereas the transition to the 5pπ state is more ambiguous, at 7.489 eV or 7.982 eV (Table S1).

Containing less π-symmetry than σ-symmetry orbitals, σ-type Rydberg orbitals should interact more strongly with the ionic core and would be characterized by a larger quantum defect δ. At this level it has also to be mentioned that rigorously, on the C_S symmetry basis, the npσ and npπ orbitals become npa' and npa" orbitals. However, assuming the molecular ion field being nearly cylindrical, i.e. diatomic-like, the σ, π-nomenclature is making sense.

The splitting between these npλ transitions is 0.082 eV for n=5 and their respective quantum defect δ=2.54 and δ=2.49 are slightly different. The same splitting observed for $H_2C_2F_2$ [24], $BrHC_2H_2$ [25], and $Br_2C_2H_2$ [3] is 0.183 eV, 0.250 eV, and 0.498 eV respectively. The 4a"→nd transitions (Fig. 4c) are observed for n=4-7. The excitation energies listed in Tables 1 and 4 correspond to transitions to Rydberg states all converging to the $IE_{ad}(\tilde{X}^2A"\text{-}BrHC_2F_2^+)$=9.695 eV [5].

The main frame of the band profile for vibrational excitation of these Rydberg transitions is made of the ν_2 (C=C stretching) vibrational mode of a' symmetry. The wavenumber associated with this vibration is measured for each transition separately. According to the Rydberg orbital-type its average value is ω_2(npσ)=1524±24 cm^{-1} (189±3 meV), ω_2(npπ)=1502±16 cm^{-1} (186±2 meV) and ω_2(nd)=1538±24 cm^{-1} (191 ±3 meV). Though being equal within experimental uncertainty, the propensity of a larger ω_2 value for nd-Rydberg states is likely to be derived. Otherwise, an overall average value $\overline{\omega}_2$=1524±20 cm^{-1} (189±3 meV) is obtained.

The wavenumber corresponding to ω_2 in the ground state of the neutral molecule is 1736 cm^{-1} [1]. The strong decrease of the wavenumber has to be linked with the depopulation of 4a"(π) involved in the Rydberg excitation, strongly weakening the C=C bond.

For all the observed Rydberg transitions involving the 4a" MO the vibrational excitation of ν_2(a') is combined with two other vibrational normal modes, i.e. ν_6(a') and ν_8(a') involving the C-Br stretching and C-F_2 rocking vibrations respectively [1]. Considering Table 4 and the average values of ω_6 and ω_8 obtained for each Rydberg state an overall averaged value $\overline{\omega}_6$=766±20 cm^{-1} (95±3 meV) and $\overline{\omega}_8$=363±20 cm^{-1} (45 ±3 meV) is derived. The corresponding wavenumbers in the ground state of the neutral molecule are ω_6= 767 cm^{-1} and ω_8= 369 cm^{-1} [1].

To carry on with the comparison of the wavenumber with the Rydberg transition-type, ω_6 is independent upon the excitation: ω_6(npσ)= 766±30 cm^{-1} (95±3 meV), ω_6(npπ)=758±16 cm^{-1} (94±2 meV) and ω_6(nd)=774±30 cm^{-1} (96±4 meV). Likely ω_8 could be significantly higher for the npσ-type transitions: ω_8(npσ)= 379±16 cm^{-1} (47±2 meV),

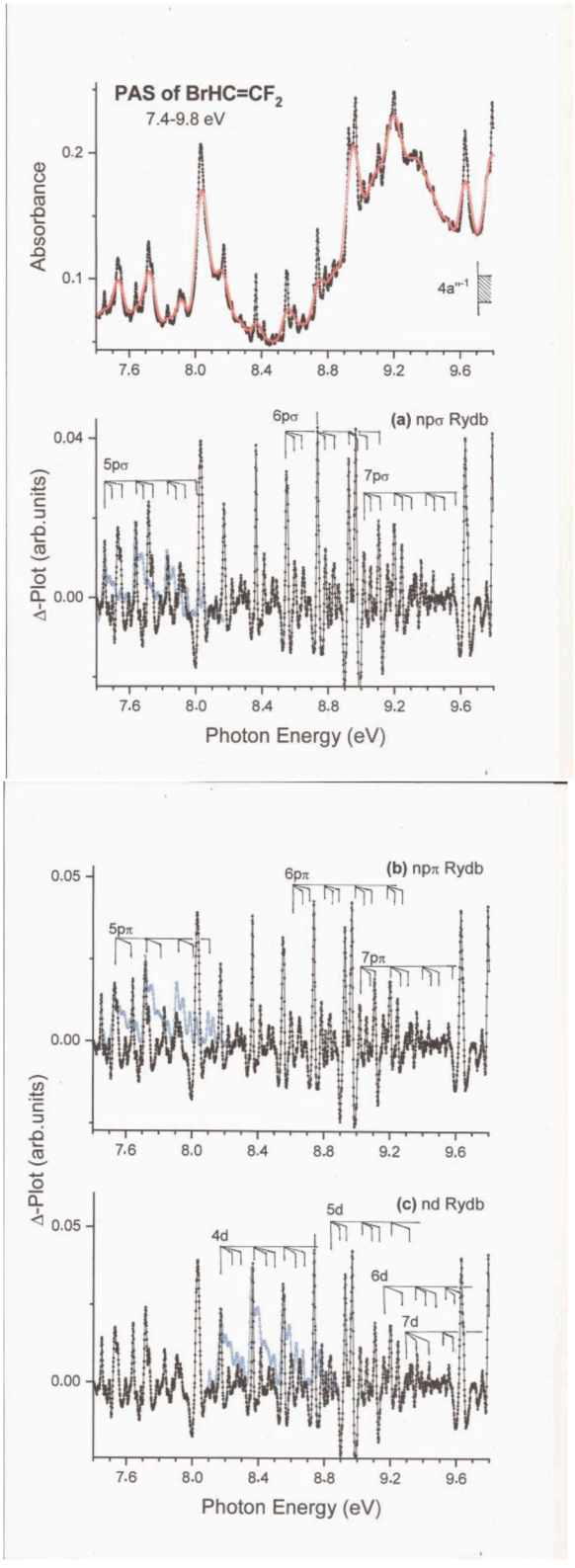

Fig. 4. Vacuum UV-PAS of $BrHC_2F_2$ between 7.5 eV and 9.7 eV photon energy (1.0 meV increments), the corresponding Δ-plot and assignments of (a) npσ (n=5-8), (b) npπ (n=5-8) and (c) nd (n=4-7)) ←4a" Rydberg transitions with their vibrational structure. The HeI-PES band of the $\tilde{X}^2$A" ionic ground state (blue open dots) of $BrHC_2F_2$ [5] is included.

Table 4
Energy positions (eV), wavenumbers (cm^{-1}) and assignments proposed for the vibrational structure of Rydberg states observed in the vacuum UV photoabsorption spectrum of $BrHC_2F_2$ between 7.4 eV and 9.5 eV and converging to the $\widetilde{X}^2A''$ ionic ground state. Conversion factor 1 eV= 8 065.545 cm^{-1} [21,22].

Converging to $IE_{ad}(\widetilde{X}^2A'')$=9.695 eV[a]			
Energy[b] (eV)	Wavenbr. (cm^{-1})	Assignment	
4a"→5pσ			
7.450	60088	**(0,0)**	ω_2=191±2 meV
7.499	60484	ν_8	1540±16 cm^{-1}
7.545	60854	ν_6	ω_6=94±2 meV
7.594	61250	$\nu_6+\nu_8$	758±16 cm^{-1}
7.642	61637	$\boldsymbol{\nu_2}$	ω_8=48±2 meV
7.691	62032	$\nu_2+\nu_8$	387±16 cm^{-1}
7.737	62403	$\nu_2+\nu_6$	
7.787	62806	$\nu_2+\nu_6+\nu_8$	
7.833	63177	$\boldsymbol{2\nu_2}$	
7.880	63556	$2\nu_2+\nu_8$	
7.927	63936	$2\nu_2+\nu_6$	
4a"→5pπ			
7.532	60750	**(0,0)**	ω_2=185±4 meV
7.626	61508	ν_6	1492±30 cm^{-1}
7.665	61822	$\nu_6+\nu_8$	ω_6=96±3 meV
7.718	62250	$\boldsymbol{\nu_2}$	774±20 cm^{-1}
7.817	63048	$\nu_2+\nu_6$	ω_8=43±3 meV
7.857	63371	$\nu_2+\nu_6+\nu_8$	347±20 cm^{-1}
7.906	63766	$\boldsymbol{2\nu_2}$	
8.001	64532	$2\nu_2+\nu_6$	
8.086	65218	$\boldsymbol{3\nu_2}$	
4a"→4d			
8.173	65920	**(0,0)**	ω_2=189±5 meV
8.220	66299	ν_8	1524±40 cm^{-1}
8.253	66565	$(2\nu_8)$	ω_6=98±3 meV
8.274	66743	ν_6	790±20 cm^{-1}
8.297	66920	na	ω_8=47±2 meV
8.321	67311	$\nu_6+\nu_8$	379±16 cm^{-1}
8.367	67484	$\boldsymbol{\nu_2}$	
8.414	67863	$\nu_2+\nu_8$	
8.467	68291	$\nu_2+\nu_6$	
8.492	68492	na	
8.551	68968	$\boldsymbol{2\nu_2}$	
[8.598]	69348	$2\nu_2+\nu_8$	
8.652	69780	$2\nu_2+\nu_6$	
8.739	70485	$\boldsymbol{3\nu_2}$	
8.786	70864	$3\nu_2+\nu_8$	
8.833	71243	$3\nu_2+\nu_6$	
4a"→6pσ			
8.557	69017	**(0,0)**	ω_2=186±3 meV
[8.598]	69348	ν_8	1500±20 cm^{-1}
[8.651]	69775	ν_6	ω_6=92±2 meV
8.739	70485	$\boldsymbol{\nu_2}$	742±16 cm^{-1}
[8.786]	70864	$\nu_2+\nu_8$	ω_8=45±2 meV
[8.832]	71235	$\nu_2+\nu_6$	363±16 cm^{-1}
[8.884]	71654	$\nu_2+3\nu_8$	
8.928	72009	$\boldsymbol{2\nu_2}$	
[8.969]	72340	$2\nu_2+\nu_8$	
[9.017]	72727	$2\nu_2+\nu_6$	
[9.060]	73074	$2\nu_2+\nu_6+\nu_8$	
4a"→6pπ			
[8.598]	69348	**(0,0)**	ω_2=188±4 meV
[8.651]	69775	ν_8	1552±30 cm^{-1}
8.696	70138	ν_6	ω_6=93±6 meV
[8.786]	70864	$\boldsymbol{\nu_2}$	768±50 cm^{-1}
8.811	71066	na	ω_8=47±5 meV
[8.832]	71235	$\nu_2+\nu_8$	388±40 cm^{-1}
8.859	71453	na	
[8.884]	71654	$\nu_2+\nu_6$	
[8.969]	72340	$\boldsymbol{2\nu_2}$	
[9.017]	72727	$2\nu_2+\nu_8$	
[9.060]	73074	$2\nu_2+\nu_6$	
[9.163]	73897	$\boldsymbol{3\nu_2}$	
[9.203]	74227	$3\nu_2+\nu_8$	
9.246	74574	$3\nu_2+\nu_6/2\nu_8$	
4a"→5d			
8.837	71275	**(0,0)**	ω_2=192±10 meV

Table 4 (*continued*)

Converging to $IE_{ad}(\widetilde{X}^2A'')$=9.695 eV[a]			
Energy[b] (eV)	Wavenbr. (cm^{-1})	Assignment	
[8.884]	71654	ν_8	1548±80 cm^{-1}
8.928	72009	ν_6	ω_6=94±5 meV
[9.017]	72727	$\boldsymbol{\nu_2}$	758±40 cm^{-1}
[9.060]	73074	$\nu_2+\nu_8$	ω_8=45±2 meV
9.107	73453	$\nu_2+\nu_6$	363±16 cm^{-1}
9.221	74372	$\boldsymbol{2\nu_2}$	
9.321	75179	$2\nu_2+\nu_6$	
4a"→7pσ			
9.004	72622	**(0,0)**	ω_2=190±6 meV
[9.107]	73453	ν_6	1532±50 cm^{-1}
[9.163]	73905	na	ω_6=99±5 meV
[9.203]	74227	$\boldsymbol{\nu_2}$	798±40 cm^{-1}
[9.246]	74574	$\nu_2+\nu_8$	$\omega 8_4$=49±6 meV
[9.300]	75010	$\nu_2+\nu_6$	395±50 cm^{-1}
[9.392]	75752	$\boldsymbol{2\nu_2}$	
[9.437]	76115	$2\nu_2+\nu_8$	
[9.486]	76510	$2\nu_2+\nu_6$	
[9.575]	77228	$\boldsymbol{3\nu_2}$	
4a"→7pπ			
[9.017]	72727	**(0,0)**	ω_2=186±3 meV
[9.060]	73074	ν_8	1500±20 cm^{-1}
[9.107]	73453	ν_6	ω_6=94±3 meV
[9.203]	74227	$\boldsymbol{\nu_2}$	758±20 cm^{-1}
[9.246]	74574	$\nu_2+\nu_8$	ω_8=42±3 meV
[9.300]	75010	$\nu_2+\nu_6$	339±20 cm^{-1}
[9.392]	75752	$\boldsymbol{2\nu_2}$	
[9.437]	76115	$2\nu_2+\nu_8$	
[9.474]	76413	$2\nu_2+2\nu_8$	
[9.486]	76510	$2\nu_2+\nu_6$	
[9.516]	76752	$2\nu_2+3\nu_8$	
[9.575]	77228	$\boldsymbol{3\nu_2}$	
4a"→6d			
9.151	73808	**(0,0)**	ω_2=187±5 meV
[9.246]	75574	ν_6	1508±40 cm^{-1}
9.331	75260	$\boldsymbol{\nu_2}$	ω_6=101±5 meV
9.437	76114	$\nu_2+\nu_8$	815±40 cm^{-1}
[9.454]	76252	$\nu_2+\nu_6$	ω_8=41±3 meV
[9.516]	76752	$\boldsymbol{2\nu_2}$	331±20 cm^{-1}
[9.554]	77058	$2\nu_2+\nu_8$	
4a"→7d			
9.320	75171	**(0,0)**	ω_2=195±3 meV
9.364	75526	ν_8	1573±20 cm^{-1}
9.411	75905	ν_6	ω_6=91±3 meV
[9.454]	76252	$3\nu_8$	734±20 cm^{-1}
[9.516]	76752	$\boldsymbol{\nu_2}$	ω_8=42±3 meV
[9.554]	77058	$\nu_2+\nu_8$	339±20 cm^{-1}

[a] Adiabatic ionization energies measured by HeI-PES [5].
[b] Energies in square brackets correspond to several assignments. Local intensities could be accounted for by the sum of those contributions.

ω_8(npπ)=355±20 cm^{-1} (44±3 meV) and ω_8(nd)=355±20 cm^{-1} (44±4 meV).

5.2.2. *Rydberg series converging to IE_{ad} ($\widetilde{A}^2A'$)=11.362 eV [5] (see Fig. 5)*

The strongest and sharpest absorptions are observed between 8.0 eV and 11.5 eV. A very crowded region is observed between 10.5 eV and 11.5 eV. In section 5.2.a several absorptions, localized in the 8.0-9.5 eV energy range, were assigned to transitions from the 4a" orbital to Rydberg states converging to IE_{ad}=9.695 eV and characterized by the highest principal quantum numbers. Excepting the strong transition at 8.033 eV, most of the strong and sharpest absorptions in the present part of the spectrum are observed between 9.2 eV and 11.0 eV as shown in Fig. 5.

This spectral region is dominated by Rydberg transitions converging to $IE_{ad}(\widetilde{A}^2A')$=11.362 eV [5]. In the HeI-PES this energy characterizes the strongest and sharpest peak of the PES. It is followed by a few weak to very weak vibrational transitions. This ionization energy has to be

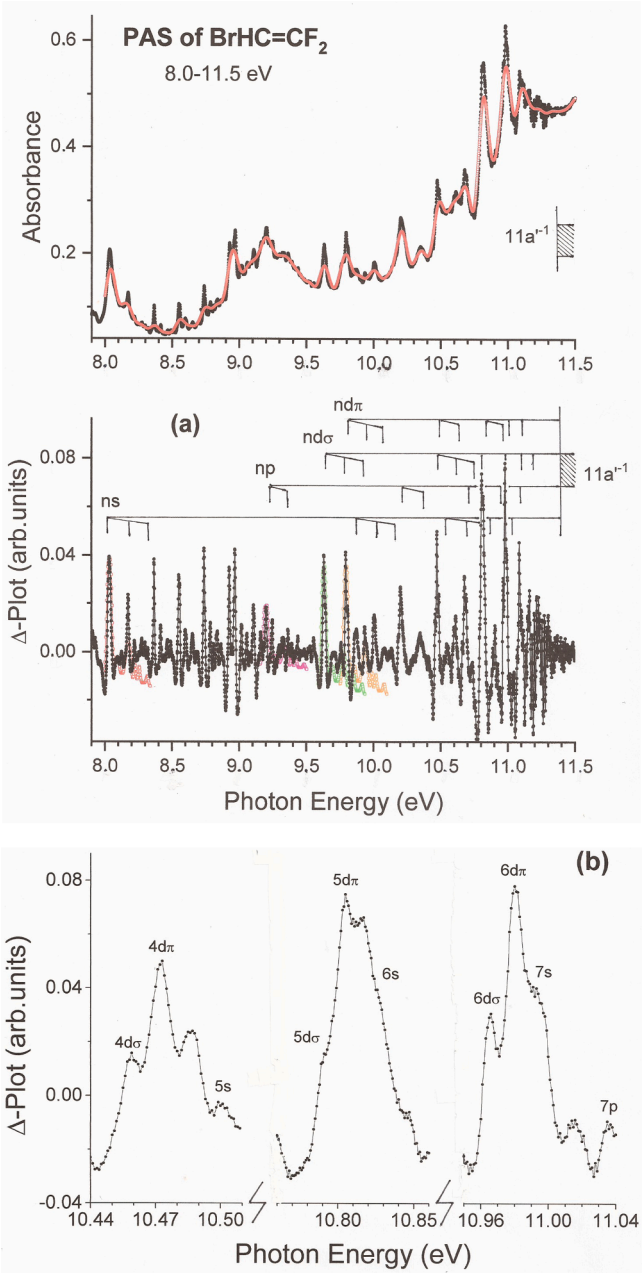

Fig. 5. Vacuum UV-PAS of $BrHC_2F_2$ between 7.9 eV and 11.5 eV photon energy (1.0meV increments), the corresponding Δ-plot and assignments of (a) ns (n=5-9), np (n=5-7), ndσ (n=4-6) and ndπ (n=4-6) ←11a' Rydberg transitions with their vibrational structure (vertical bars). The HeI-PES band of the $\tilde{A}^2$A' first ionic excited state (red, magenta, green and orange open dots) of $BrHC_2F_2$ [5] is included . (b) Absorption bands at 10.473 eV, 10.805 eV and 10.979 eV on an expanded energy scale and location of indicated Rydberg transitions.

assigned to the ionization of the Br atom non-bonding lone-pair (11a') MO [5].

The analysis of the present spectral region provides several Rydberg transitions listed in Table 1: from the 11a' MO transitions to ns (n=5-9 and with $\bar{\delta}$=2.97±0.03), np (n=5-9 and with $\bar{\delta}$=2.49±0.06) and ndλ (n=4-8(9)) Rydberg orbitals. For λ=0(σ) $\bar{\delta}$=1.16±0.04 and λ=1(π) $\bar{\delta}$=1.07±0.05. Several very sharp multiplet-absorption bands observed in the region between 10.4 eV and 11.0 eV are displayed on an expanded energy scale in Fig.5b, showing the higher term Rydberg transitions.

As shown in Table S1, several 11a'→nlλ transitions are obtained by quantum chemical calculations. For several transitions a fairly good correlation between predicted and experimental energy values could be mentioned.

For the first members of these series the vibrational structure could be determined using the Franck-Condon profile of the second HeI-PES band corresponding to the $\tilde{A}^2$A' ionic state [5] and reproduced in Fig. 5a. The result of this analysis is shown in Table 5 together with the assignments proposed in the present work. For the first members of all the series two vibrational wavenumbers are observed and are related to the vibrational motions ν_4(a') (C-F symmetric stretching) and ν_8(a') (CF_2 rocking). The values of the wavenumbers ω_4 and ω_8 measured for nine individual Rydberg transitions are listed in Table 5. As averaged over the nine measurements $\bar{\omega}_4$=1121±40 cm^{-1} (139±5 meV) and $\bar{\omega}_8$=363±50 cm^{-1} (45±6 meV). These wavenumbers have to be compared with those

Table 5
Energy positions (eV), wavenumbers (cm^{-1}) and assignments proposed for the vibrational structure of Rydberg states observed in the vacuum UV photo-absorption spectrum of $BrHC_2F_2$ between 8.0 eV and 11.5 eV and converging to the $\tilde{A}^2$A' first ionic excited state. Conversion factor 1 eV= 8 065.545 cm^{-1} [21, 22].

Converging to IE_{ad}=11.362 eV			
Energy (eV)	Wavenbr. (cm-1)	Assignment	
11a'→5s			
8.033	64791	**(0,0)**	ω_4=144±4 meV
8.173	65920	ν_4	1160±30 cm^{-1}
8.222	66315	$\nu_4+\nu_8$	ω_8=51±3 meV
8.276	66750	$\nu_4+2\nu_8$	410±20 cm^{-1}
8.321	67113	$2\nu_4$	
11a'→5p			
9.200	74203	**(0,0)**	ω_4=133±2 meV
9.247	74582	ν_8	1073±16 cm^{-1}
9.299	75002	$2\nu_8$	ω_8=44±10 meV
9.333	75276	ν_4	355±80 cm^{-1}
9.364	75526	$\nu_4+\nu_8$	
11a'→4dσ			
9.631	77679	**(0,0)**	ω_4=138±4 meV
9.713	78340	$2\nu_8$	1113±30 cm^{-1}
9.765	78760	ν_4	ω_8=44±2 meV
9.807	79099	$\nu_4+\nu_8$	355±16 cm^{-1}
9.908	79913	$2\nu_4$	
11a'→4dπ			
9.795	79002	**(0,0)**	ω_4=141±2 meV
9.846	79413	ν_8	1137±16 cm^{-1}
9.935	80131	ν_4	ω_8=50±2 meV
9.985	80534	$\nu_4+\nu_8$	403±16 cm^{-1}
10.071	81228	$2\nu_4$	
11a'→6s			
9.874	79639	**(0,0)**	ω_4=132±4 meV
10.006	80704	ν_4	1065±30 cm^{-1}
10.081	81309	$\nu_4+2\nu_8$	ω_8=38±4meV
10.139	81777	$2\nu_4$	306±30 cm^{-1}
11a'→6p			
10.203	82293	**(0,0)**	ω_4=143±2 meV
10.346	83446	ν_4	1153±16 cm^{-1}
11a'→5dσ			
10.459	84358	**(0,0)**	ω_4=139±2 meV
10.499	84680	ν_8	1121±16 cm^{-1}
10.598	85479	ν_4	ω_8=40±2 meV
10.636	85785	$\nu_4+\nu_8$	323±16 cm^{-1}
10.736	86592	$2\nu_4$	
11a'→5dπ			
10.473	84470	**(0,0)**	ω_4=138±2 meV
10.526	84898	ν_8	1113±16 cm^{-1}
10.611	85583	ν_4	ω_8=54±4 meV
10.636	85801	na	435±30 cm^{-1}
10.666	85987	$\nu_4+\nu_8$	
11a'→6dπ			
10.805	87148	**(0,0)**	ω_4=147±2 meV
10.845	87471	ν_8	1186±16 cm^{-1}
10.889	87971	$2\nu_8$	ω_8=42±4 meV
10.952	88334	ν_4	339±30 cm^{-1}

a Adiabatic ionization energy measured by HeI-PES [5].

determined in the neutral ground state of $BrHC_2F_2$ [1], i.e. ω_4= 1172 cm^{-1} and ω_8= 369 cm^{-1}.

5.2.3. Rydberg series converging to $IE_{vert}(\tilde{B}^2A'')$=12.59 eV [5] and $IE_{vert}(\tilde{C}^2A')$=14.48 eV [5] (see Fig.6)

The spectral region between 11.0 eV and 12.5 eV is very congested and densely occupied by long series of high frequency modulations as shown in

Fig.6. It could be divided in two quite different parts made of (i) a series of fairly strong and very sharp oscillations extending between 11.05 eV and 11.44 eV and (ii) a long series of weak or very weak oscillations between 11.48 eV and 12.50 eV displayed in Fig. 6a. For easiness of its analysis the region between 11.0 eV and 11.4 eV has been recorded with 0.2 meV energy increments and is reproduced in Fig. 6b. The corresponding Δ-plot is displayed in Fig. 6c.

In Table 6a are listed the energy positions recorded for the energy range of 11.066 eV to 11.442 eV. An average spacing of about 16 meV (~130 cm^{-1}) is observed over the whole energy range. However, a closer examination of the absorption spectrum points to at least five groups of peaks. These are better discerned in the FFT-smoothed spectrum shown in Fig. 6b (red open dots).

An attempt for classification and assignments are proposed in Table 6a where two vibrational modes should be involved, i.e. ν_7(a') (CF_2 deformation) and ν_9(a') (BrHC rocking). The corresponding wavenumbers should be ω_7= 508±24 cm^{-1} (63±3 meV) and ω_9=130 ±16 cm^{-1} (16±2 meV). This description is based on the comparison of these wavenumber values with those determined in the neutral molecular ground state, i.e. ω_7=568cm^{-1} and ω_9=164 cm^{-1} [1].

The Rydberg state excited in this transition should involve an (anti)-bonding MO allowing a considerable change of geometry, weakening both ends of the molecule. It should also converge to an ionic excited state showing similar properties. The first ionized state of $BrHC_2F_2$, characterized by a broad HeI-PES band, has been measured at $IE_{vert}(\tilde{B}^2A'')$=12.59 eV [5] spreading between 12.4 eV and 13.2 eV. Using the Rydberg relation (1) and the vertical excitation of 11.2 eV a term value T=1.4 eV is obtained, providing n*=3.12 and δ=2.88 characterizing a 4d/6s-type Rydberg series [23].

Above 11.44 eV and up to 12.5 eV the absorption spectrum exhibits a long series of very weak and regularly spaced features of variable intensities. These are better highlighted in the Δ-plot displayed in Fig. 6a. Measuring the interval between the successive features observed in the entire energy range an average value of about 40±5 meV (323±40 cm^{-1}) is obtained. This wavenumber best corresponds to ν_8 (CF_2 rocking) vibration when compared to its value of 369 cm^{-1} in the ground state of the neutral molecule [1].

However, a closer examination of this region would lead to the existence of at least two progressions differing by the intensity and the width of their components. On this basis two Rydberg transitions could be invoked with E_{exc}^{vert}≈11.6 eV and E_{exc}^{vert}≈12.2 eV successively. The energy position of the features corresponding to each series is listed in Table 6b and 6c. Both progressions show a wavenumber of about 325 cm^{-1} (40 meV). For both involved Rydberg states E_{exc}^{vert} lies below, but close to, $IE_{vert}(\tilde{B}^2A'')$=12.59 eV. The next higher energetic ionized states are measured at $IE_{vert}(\tilde{C}^2A')$=14.48 eV [5] and $IE_{vert}(\tilde{D}^2A'')$=15.62 eV [5]. Both ionic states exhibit broad photoelectron bands [5].

The convergence of the Rydberg states at E_{exc}^{vert}≈11.6 eV and 12.2 eV towards the ionized state at 12.59 eV would require exhibiting about the same structure as the lower lying Rydberg state at E_{exc}^{vert}≈11.2 eV. This state shows a progression of ν_7 (ω_7=508 cm^{-1}) combined with ν_9 (ω_9=130 cm^{-1}). None of these wavenumbers are observed in the vibrational progressions observed at E_{exc}^{vert}≈11.6 eV and 12.2 eV.

In the first order interpretation, using relation (1) and fixing the convergence limit at $IE_{vert}(\tilde{C}^2A')$=14.48 eV [5], term values of T≈2.9 eV and T≈2.3 eV are obtained for these Rydberg states respectively. The observed term value of T≈2.9 eV would provide n*=2.17 and δ=2.83.

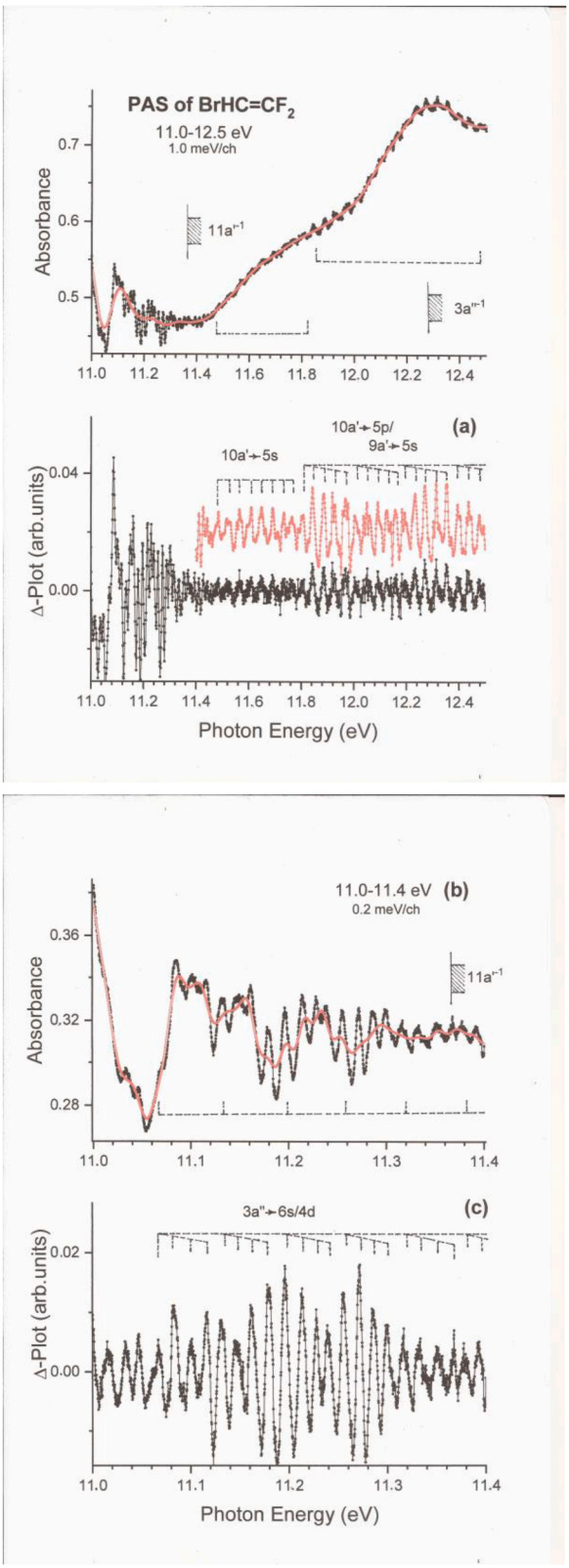

Fig. 6. Vacuum UV-PAS of $BrHC_2F_2$ (a) between 11.0 eV and 12.5 eV photon energy (1.0 meV increments) and the corresponding Δ-plot and tentative assignments. (b) The 11.0-11.4 eV region on an expanded energy scale with 0 .2 meV increments and (c) the corresponding Δ-plot and tentative assignments. Vertical bares show the proposed vibrational structure.

Table 6
Energy positions (eV), wavenumbers (cm^{-1}) and assignments proposed for the vibrational structure of Rydberg states observed in the vacuum UV photo-absorption spectrum of $BrHC_2F_2$ between 11.0 eV and 12.5 eV and converging to the $\tilde{B}^2A$" and $\tilde{C}^2A$' ionic excited states. Conversion factor 1 eV= 8 065.545 cm^{-1} [21,22].

(a)			
Converging to IE_{vert}=12.59 eV[a]			
Energy (eV)	Wavenbr. (cm-1)	Assignment	
11.066	89286	**(0,0)**	
11.083	89390	ν_9	ω_7=63±3 meV
11.099	89519	$2\nu_9$	508±20 cm^{-1}
11.116	89657	$3\nu_9$	
11.130	89786	$\boldsymbol{\nu_7}$	ω_9=16±2 meV
11.146	89899	$\nu_7+\nu_9$	130±16 cm^{-1}
11.161	90020	$\nu_7+2\nu_9$	
11.179	90165	$\nu_7+3\nu_9$	
11.196	90302	$\boldsymbol{2\nu_7}$	
11.213	90439	$2\nu_7+\nu_9$	
11.228	90560	$2\nu_7+2\nu_9$	
11.239	90649	$2\nu_7+3\nu_9$	
11.254	90770	$\boldsymbol{3\nu_7}$	
11.271	90907	$3\nu_7+\nu_9$	
11.284	91012	$3\nu_7+2\nu_9$	
11.299	91133	$3\nu_7+3\nu_9$	
11.316	91270	$\boldsymbol{4\nu_7}$	
11.333	91407	$4\nu_7+\nu_9$	
11.350	91544	$4\nu_7+2\nu_9$	
11.367	91681	$4\nu_7+3\nu_9$	
11.379	91778	$\boldsymbol{5\nu_7}$	
11.392	91883	$5\nu_7+\nu_9$	
11.411	92173	$5\nu_7+2\nu_9$	
11.428	92036	$5\nu_7+3\nu_9$	
11.442	92286	$\boldsymbol{6\nu_7}$	
(b)			
11.486	92600	**(0,0)**	(ω_2=205 meV
11.522	92923	ν_8	1653 cm^{-1})
11.564	93278	$2\nu_8$	ω_8=41±4 meV
11.611	93617	$3\nu_8$	330±30 cm^{-1}
11.648	93956	$4\nu_8$	
11.691	94310	$(5)\nu_8/(\boldsymbol{\nu_2})$	
11.734	94641	$(6)\nu_8+(\nu_2)$	
11.776	94875	$(7)\nu_8+(\nu_2)$	
(c)			
Converging to IE_{vert}=14.48 eV [a]			
Energy (eV)	Wavenbr. (cm-1)	Assignment	
11.805	95190	**(0,0)**	ω_8=40±5 meV
11.841	94504	ν_8	320±40 cm^{-1}
11.883	95843	$2\nu_8$	(ω_2=197±4 meV
11.919	96133	$3\nu_8$	1590±30 cm^{-1})
11.969	96537	$4\nu_8$	
12.002	96803	$\boldsymbol{(\nu_2)}/5\nu_8$	
12.051	97212	$(6)\nu_8+(\nu_2)$	
12.090	97512	$(7)\nu_8+(\nu_2)$	
12.126	97803	$(8)\nu_8+(\nu_2)$	
12.162	98093	$(9)\nu_8+(\nu_2)$	
12.195	98359	$\boldsymbol{(2\nu_2)}/10\nu_8$	
12.234	98674	$(11)\nu_8+(2\nu_2)$	
12.269	98956	$(12)\nu_8+(2\nu_2)$	
12.313	99311	$(13)\nu_8+(2\nu_2)$	
12.355	99650	$(14)\nu_8+(2\nu_2)$	
12.395	99972	$\boldsymbol{(3\nu_2)}/15\nu_8$	
12.434	100287	$(16)\nu_8+(3\nu_2)$	
12.480	100658	$(17)\nu_8+(3\nu_2)$	

[a] Vertical ionization energy measured by HeI-PES [5].

These values of n* and δ will point to a 10a'→5 s Rydberg transition for the progression with E_{exc}^{vert}≈11.6 eV. By the same way, the term value of T=2.3 eV, yielding n*=2.43 and δ=2.52 for the 10a'→5p Rydberg transition, is assigned to the progression observed at E_{exc}^{vert}≈12.2 eV.

As already mentioned, both vibrational progressions are dominated by energy spacing of about 40 meV. In Tables 6b and 6c a first possible assignment to the structure observed in both Rydberg states is the occurrence of the single ν_8 (CF_2 rocking) vibrational mode with 7 to 17 harmonics.

A closer examination of the second progression between 11.8 eV and 12.5 eV could reveal periodic intensity variations as suggested in Fig. 5a. As shown in Table 6b and 6c, the features observed in this energy range could alternatively be arranged by ν_2 (C=C stretching) combined with ν_8 vibrations: ω_2=1590±30 cm^{-1} (197±4 meV) and ω_8=320±40 cm^{-1} (40 ±5 meV) are measured. For the shorter progression observed between 11.48 eV and 11.78 eV ω_2=1653 cm^{-1} (205 meV) and ω_8=330±30 cm^{-1} (41±4 meV) are obtained.

Furthermore, an alternative assignment of the second progression between 11.8 eV and 12.5 eV is to consider the convergence to the $IE_{vert}(\tilde{D}^2A")$ =15.62 eV which cannot be discarded. In that case a term value of T=3.4 eV is obtained, providing n*=1.99 and δ=3.01 and likely corresponding to 9a'→5 s Rydberg transition.

5.2.4. *Rydberg series converging to IE_{vert}= 15.62-16.14 eV [5] (see Fig. 7)*

The vacuum UV-PAS of $BrHC_2F_2$ between 12.0 eV and 15.0 eV has been recorded with 10 meV increments only. The result is displayed in Fig. 7 (upper panel). This part of the spectrum is made of four broad absorption bands with a maximum at 12.23 eV, 13.0 eV, 13.92 eV and 14.6 eV successively. The Δ-plot, obtained by subtraction of 75 points FFT-smoothing (blue open circle), is shown in Fig. 7 (lower panel, blue dots).

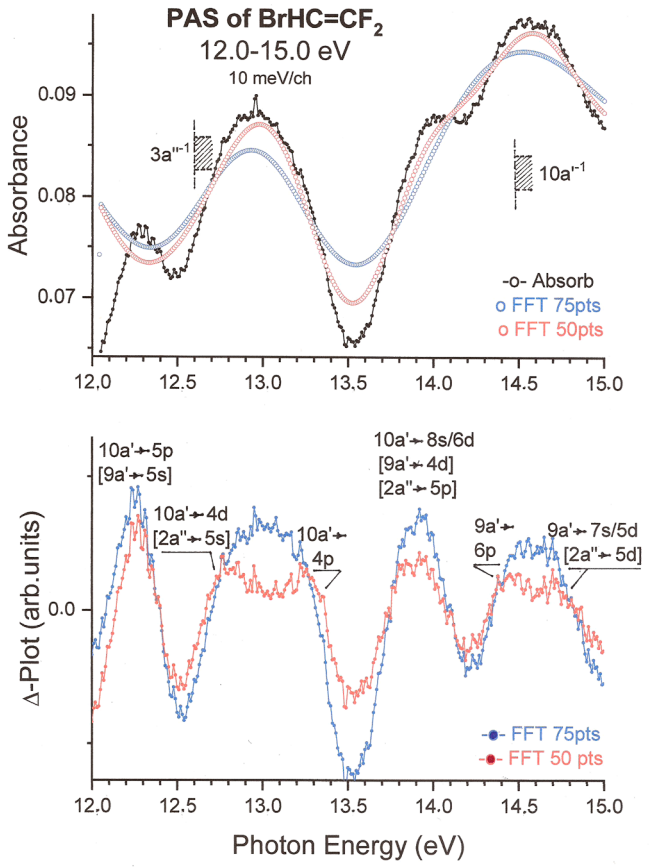

Fig. 7. Vacuum UV-PAS of $BrHC_2F_2$ between 12 eV and 15 eV photon energy measured with 10 meV increments: (upper panel) absorbance (black solid circle) and FFT smoothing including 75 points (blue open circle) and 50 points (red open circle). Dashed vertical bars locate vertical ionization limits; (lower panel) the corresponding Δ-plots for FFT 75 points (bleu dots) and FFT 50 points (red dots).

For the two bands at 12.23 eV and 13.92 eV a regular structure is distinctly apparent. That of the former has already been analyzed in section 5.2.c. Despite the present recording conditions (10 meV increments) the ν_8 (CF_2 rocking) progression remains clearly visible as shown in Fig. 7 and listed in Table S4a: the first and fourth columns list the measurements under the two (1.0 meV and 10 meV increments) recording conditions.

For the absorption band with its maximum at 13.92 eV the energy position of the series of features is listed in Table S4b. The average spacing of 310±30 cm^{-1} (38±4 meV) is in good agreement with that measured for the band at 12.23 eV (320±40 cm^{-1}). Furthermore, the profile of the two bands is rather close. These observations would argue for assigning the band at 13.92 eV to be a member of a series converging to IE_{vert}=14.48 eV [5]. Using relation (1) a term value of T=0.56 eV is deduced and n*=4.93 providing δ values of 3.07 and 1.07 assigned to 10a'→ 8s/6d Rydberg transitions.

In addition, higher lying convergence limits are formally possible and have to be mentioned at IE_{vert}=15.62 eV [5] and at IE_{vert}=16.14 eV [5]. To both ionization energies corresponds a broad HeI-PES doublet-band [5]. Considering the absorption band at 13.92 eV, term values T=1.7 eV and T=2.2 eV are obtained respectively. These term values provide n*=2.83 (δ=1.17) and n*=2.47 (δ=2.53) respectively and should correspond to 9a'→4d and 2a"→5p Rydberg transitions. A univocal assignment is not allowed with the present data set.

In the presently considered photon energy range two strong bands are observed, about twice as broad as those measured at 12.23 eV and at 13.92 eV. Their maxima are fairly flat and their position could only be estimated roughly at about 13.0 eV and 14.6 eV.

For a deeper analysis of these two bands a slightly different subtraction procedure has been applied by using the fast Fourier transform (FFT) smoothing including 50 points (see Fig. 7, upper panel, red open dots) instead of 75 points (see Fig. 7, upper panel, blue open dots). Its subtraction from the absorbance curve gives rise to the Δ-plot shown in Fig. 7 (red plot in lower panel). This procedure leads to show that each broad band could at least be made up of two separate narrower subbands. The four resulting bands have their maximum at 12.81 eV and 13.25 eV and at 14.44 eV and 14.72 eV successively. In Tables S4c and S4d are listed the features noted in these bands. Because of lack of any indication of interaction between Rydberg states a first order interpretation would allow us to attempt an assignment to these bands.

Considering the sub-band at E_{exc}^{vert}=12.81 eV likely only the convergence limits at IE_{vert}=14.48 eV [5] and 16.14 eV [5] have to be considered. On the basis of the term values T=1.67 eV and T=3.33 eV respectively, possible Rydberg transitions 10a'→4d (with n*=2.85 and δ=1.15) and 2a"→5 s (with n*=2.02 and δ=2.98) are obtained successively. The convergence limit at 15.62 eV likely has to be discarded, the term value being T=2.81 eV (with n*=2.20 and δ=2.80) assigned to 9a'→5 s. It has to be noticed that the 9a'→5 s Rydberg transition was already mentioned as probable assignment to the 12.2 eV band.

For the sub-band at E_{exc}^{vert}=13.25 eV only the convergence limit at IE_{vert}=14.48 eV should be considered. The term value T=1.23 eV (with n*=3.32 and δ=2.68) is close to the value predicted at T=1.11 eV [23] for the 10a'→6p Rydberg transition.

At this point it could be stressed that the four absorption bands at E_{exc}^{vert}=12.23 eV, 12.81 eV, 13.25 eV and 13.92 eV are likely related. They could be the 5p-, 4d-, 6p- and 8s/6d-members of a Rydberg series converging to the same limit at IE_{vert}=14.48 eV [5]. Furthermore, Table 6c and Table S4 a-c list the energy position of the possible structures observed in these bands. These all show one reproducible spacing of 320 cm^{-1} (40 meV) likely corresponding to the wavenumber characterizing the ν_8 (CF_2 rocking) vibrational mode.

The two highest energy sub-bands at E_{exc}^{vert}=14.44 eV and 14.72 eV have to be assigned to excitations to Rydberg states converging to higher-lying ionization continua, i.e. IE_{vert}=15.62 eV [5] and 16.14 eV [5].

The most probable assignment of the first band at E_{exc}^{vert}=14.44 eV corresponds to the 9a'→6p Rydberg transition: a term value T=1.18 eV (with n*=3.39 and δ=2.60) is obtained for the convergence limit at 15.62 eV. This value is close to T=1.11 eV predicted [23] for this transition. Table S4 d lists the energy positions of the possible structure detected in this band. An average spacing of 290±80 cm^{-1} (36±10 meV) is obtained. This wavenumber is lower than ω_8=369 cm^{-1} but higher than ω_9=164 cm^{-1} observed for the neutral in the infrared spectrum [1].

The interpretation of the absorption band at E_{exc}^{vert}=14.72 eV is more ambiguous. Term values of T=0.90 eV and T=1.42 eV are obtained considering the convergence limits at IE_{vert}=15.62 eV [5] and 16.14 eV [5] respectively. Both these term values are close to T=0.85 eV and T=1.51 eV predicted [23] for 9a'→7s/5d and 2a"→5s/4d Rydberg transitions. As shown in Table S4 d the average spacing measured for the structure of this band is 380±70 cm^{-1} (47±9 meV).

6. Conclusions

For the first time the vacuum UV photoabsorption spectrum of $BrHC{=}CF_2$ has been measured between 5 eV and 15 eV using synchrotron radiation and has been analyzed in detail. Quantum chemical calculations have been performed on the neutral ground state and several excited states of the title molecule to support the proposed assignments.

At low energy several valence→valence transitions have been detected between 5.0 eV and 6.3 eV. A well defined $\pi_{CC}\rightarrow\pi_{CC}^*$ valence transition is observed at E_{vert}= 6.955 eV showing a well defined vibrational structure. A very weak π→5 s Rydberg transition is likely occurring at E_{vert}=6.43 eV. At this point, the fluorination, bromination and the mixed bromo-fluorination effects on the C=C bond strength and excitation can be evaluated and compared as shown in Table 7.

Above 7 eV and up to 10.8 eV many transitions are pointed out involving fairly long ns-, npλ- and ndλ- Rydberg series converging to the first two adiabatic ionization continua at IE_{ad}= 9.695 eV and 11.362 eV [5]. Their vibrational structure has been analyzed and assignments are proposed. Above 11.0 eV and up to 15 eV the spectrum is made of (i) strong very sharp transitions between 11.06 eV and 11.44 eV and (ii) long series of weak to very weak modulations superimposed on broad strong bands. These features are tentatively assigned to vibrational progressions of several Rydberg states, members of series converging to higher lying excited states of the $BrHC{=}CF_2^+$ ion. The fate of these neutral highly excited states will be analyzed in detail by dissociative ionization experiments reported in a forthcoming paper [5].

At this point of the systematic analyses of the vacuum UV-PAS of halogenated derivatives of ethylene, detailed comparisons can be made. These are important for atmospheric chemistry related issues such as the calculation of ozone depleting potential (ODP) [2] for these chemicals and the search for tradeoffs of refrigerants of low global warming potentials (GWP's) [26].

The vacuum UV-PAS of $H_2C_2F_2$ [24], $Br_2C_2F_2$ [3] and $BrHC_2F_2$, investigated in the present work, are compared in the photon energy ranges of 5 eV to 15 eV (Fig. 8a) and 5 eV to 8 eV (Fig. 8b). Remarkably,

Table 7
Evolution of the excitation energy (E_{vert}/eV) and wavenumber of the=C bond stretching (ω_e/cm^{-1}) associated with the $\pi_{CC}\rightarrow\pi_{CC}^*$ valence transition in ethylene, fluorine and/or bromine- and bromo-fluoro- substituted ethylenes.

Molecule	E_{exc} ($\pi_{CC}\rightarrow\pi_{CC}^*$) (eV)		ω_e(C=C)	Ref.
	adiab.	vert.	(cm^{-1})	
[$H_2C{=}CH_2$]	[7.08]	[7.602]	[1320]	[11]
[$H_2C{=}CHF$]	[6.892]	[7.644]	-	[11]
$H_2C{=}CF_2$	6.742	7.482	1475	[24]
$BrHC{=}CF_2$	6.756	6.955	1548	pw
$Br_2C{=}CF_2$	6.595	6.920	1315	[4]
$Br_2C{=}CH_2$	6.231	6.231	1378	[3]
[$BrHC{=}CH_2$]	[~5.9]	[6.473]	-	[25]

a In square brackets: ethylene and mono-substituted ethylenes.
b pw" stays for "present work"

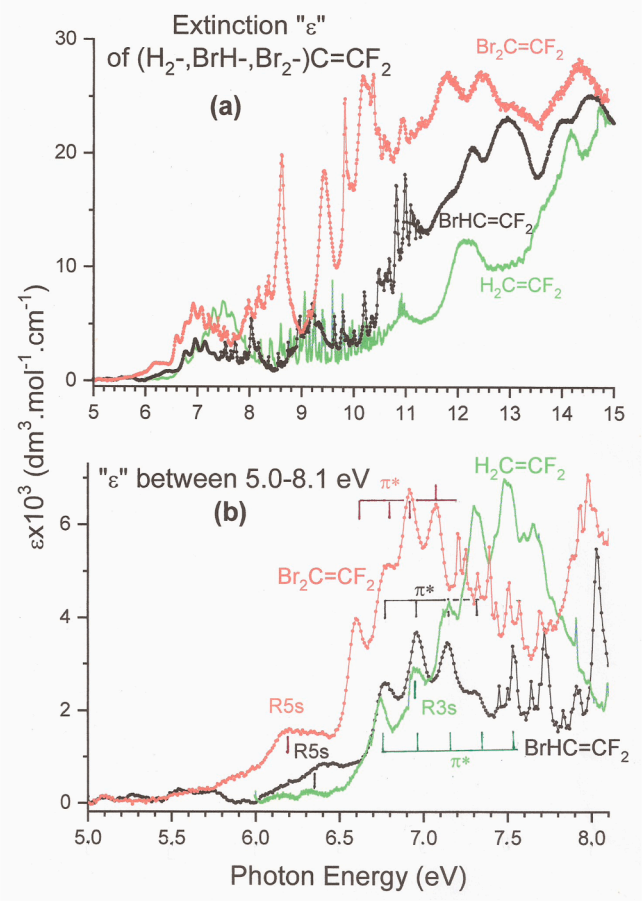

Fig. 8. Comparison of the vacuum UV photoabsorption spectra of $BrHC_2F_2$ (black dots), $Br_2C_2F_2$ (red dots) and $H_2C_2F_2$ (green dots) between (a) 5 eV and 15 eV (b) 5.0 eV and 8.1 eV photon energy.

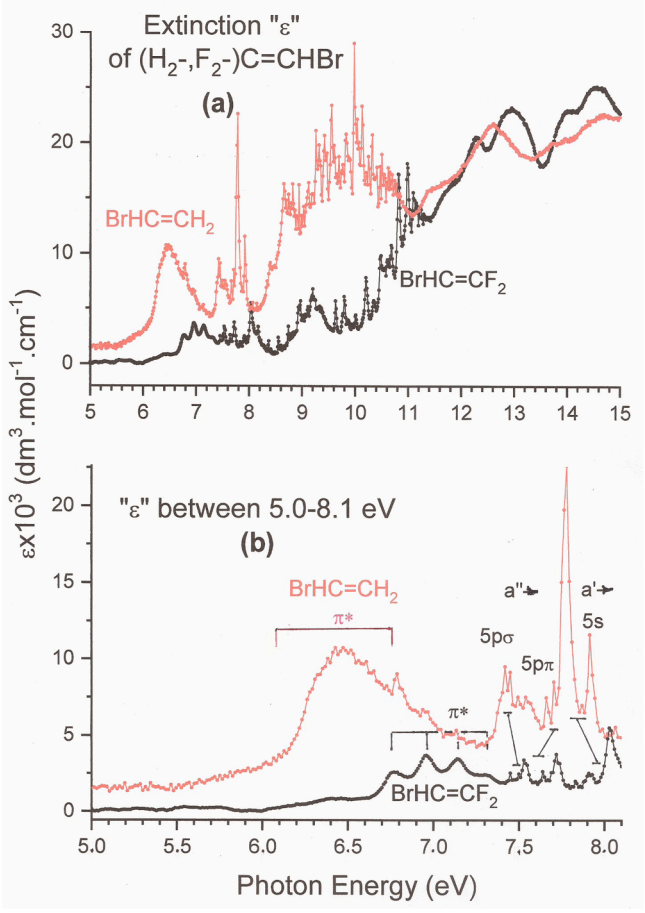

Fig. 9. Comparison of the vacuum UV photoabsorption spectra of $BrHC_2F_2$ (black dots) and $BrHC_2H_2$ (red dots) between (a) 5 eV and 15 eV (b) 5.0 eV and 8.1 eV photon energy.

the extinction coefficient $\varepsilon_{h\nu}$ considerably differ between 8 eV and 15 eV; $\varepsilon_{h\nu}(H_2C_2F_2) << \varepsilon_{h\nu}(BrHC_2F_2) << \varepsilon_{h\nu}(Br_2C_2F_2)$. Contrarily, in the low photon energy range of 5 eV to 8 eV, $\varepsilon_{h\nu}(BrHC_2F_2) < \varepsilon_{h\nu}(H_2C_2F_2) \approx \varepsilon_{h\nu}(Br_2C_2F_2)$. Furthermore, the adiabatic $\pi_{CC} \rightarrow \pi_{CC}^*$ valence transition energy is only slightly shifting $Br_2C_2F_2 < H_2C_2F_2 \leq BrHC_2F_2$, i.e. at 6.595 eV [3], 6.742 eV [24] and 6.756 eV successively. Orkin et al. [2] and Howard [27] measured the hydroxyl radical reaction rates at 298 K being $2.0*10^{-12}$ $cm^3.mol^{-1}.s^{-1}$ toward $H_2C_2F_2$ [24] and $4.5*10^{-12}$ $cm^3.mol^{-1}.s^{-1}$ toward $BrHC_2F_2$ [2].

The drastic "fluorination effect" on the vacuum UV-PAS of $BrHC_2H_2$ is illustrated in Fig. 9. The extinction $\varepsilon_{h\nu}$ being rather close for both $BrHC_2H_2$ and $BrHC_2F_2$ in the 11 eV to 15 eV photon energy range (see Fig. 9a), a much higher extinction is observed for $BrHC_2H_2$ between 5 eV and 10 eV. This latter observation is valid for the $\pi_{CC} \rightarrow \pi_{CC}^*$ valence transition (see Fig. 9b): $\varepsilon_{h\nu}(BrHC_2F_2) << \varepsilon_{h\nu}(BrHC_2H_2)$ and their vertical transition energy are strongly shifted, i.e. 6.40 eV [25] and 6.955 eV. Perry et al. [28] and Orkin et al. [2] measured the hydroxyl radical reaction rates at 298 K being $4.5*10^{-12}$ $cm^3.mol^{-1}.s^{-1}$ for $BrHC_2F_2$ and $7.0*10^{-12}$ $cm^3.mol^{-1}.s^{-1}$ for $BrHC_2H_2$.

CRediT authorship contribution statement

R. Locht: Writing – original draft, Funding acquisition, Data curation, Conceptualization. **C. Kune:** Software.

Declaration of competing interest

The authors declare that they have no known competing financial interests or personal relationships that could have appeared to influence the work reported in this paper.

Acknowledgment

We acknowledge the European Community for its financial support to the access to the BESSY II large-scale facility through the contract n° R II 3 CT-2004-506008.

Supplementary materials

Supplementary material associated with this article can be found, in the online version, at doi:10.1016/j.jqsrt.2025.109654.

Data availability

The data that has been used is confidential.

References

[1] Theimer R, Nielsen JR. J.Chem.Phys 1957;37:264.
[2] Orkin VL, Louis F, Huie RE, Krylo MJ. J.Phys.Chem 2002;A 106:10195.
[3] Locht R, Dehareng D. J.Quant.Spect.Rad.Trans 2023;305:108626.
[4] Locht R, Dehareng D. J.Quant.Spect.Rad.Trans 2023;306:108640.
[5] Locht R., Kune C, *unpublished results.*
[6] Locht R, Dehareng D, Leyh B. Mol.Phys 2014;112:1520.
[7] Marmet P. Rev. Sci.Instrum. 1979;50:79.
[8] Carbonneau R, Bolduc E, Marmet P. Can.J.Phys. 1973;51:505.
[9] Carbonneau R, Marmet P. Can.J. Phys. 1973;51:2203.
[10] ibid. *Phys.Rev. A* 1974;9:1898.

[11] Locht R, Leyh B, Dehareng D, Jochims H-W, Baumgärtel H. Chem.Phys. 2009;362:97.
[12] Locht R, Dehareng D, Leyh B. J.Phys. B At. Mol.Opt.Phys. 2012;45:115101.
[13] Lofthus A, Krupenie PH. J.Phys.Chem.Ref.Data 1977;6:113.
[14] Frisch MJ, Trucks GW, Schlegel HB, Scuseria GE, M A, Robb MA, Cheeseman JR, Scalmani G, Barone V, Petersson GA, Nakatsuji H, Caricato M, Li X, Marenich A, Bloino J, Janesko G, Gomperts R, Mennucci B, Hratchian HP, Ortiz JV, Izmaylov AF, Sonnenberg JL, Williams G, Young F, Ding F, Lipparini F, Egidi F, Goings J, Peng B, Petrone A, Henderson T, Ranasinghe D, Zakrzewski VG, Gao J, Rega N, Zeng G, Liang W, Hada M, Ehara M, Toyota K, Fukuda R, Hasegawa J, Ishida M, Nakajima T, Honda Y, Kitao O, Nakai H, Vreven T, Throssell K, Montgomery Jr JA, Peralta JE, Ogliaro F, Bearpark M, Heyd JJ, Brothers E, Kudin KN, Staroverov VN, Keith T, Kobayashi R, Normand J, Raghavachari K, Rendell A, Burant JC, Iyengar SS, Tomasi J, Cossi M, Millam JM, Klene M, Adamo C, Cammi R, Ochterski JW, Martin RL, Morokuma K, Farkas O, Foresman JB, Fox DJ. Gaussian 09. Wallingford CT: Gaussian, Inc.; 2016. Revision D.01.
[15] Krishnan R, Binkley JS, Seeger R, Pople JA. J.Chem.Phys 1980;72:650.
[16] Dunning Jr TH. J.Chem.Phys 1989;90:1007.
[17] Zhao Y, Truhlar DG. Theor.Chem.Acc 2008;120:215.
[18] Van Caillie C, Amos RD. Chem.Phys.Letters 2000;317:159.
[19] Becke AD. J.Chem.Phys 1993;98:5648.
[20] Stephens PJ, Devlin FJ, Chabalowski C F, Frisch MJ. J.Phys.Chem 1994;98:11623.
[21] Tiesinga E, Mohr PJ, Newell DB, Taylor BN. J.Phys.Chem.Ref.Data 2021;50:033105.
[22] Mohr PJ, Newell DB, Taylor BN. Rev.Mod.Phys. 2016;88:035009.
[23] Robin MB. Higher Excited States of Polyatomic Molecles, I. New York: Academic Press; 1974. p. 51. 1975 *ibid.* Vol.II pp 50.
[24] Locht R, Jochims H-W, Leyh B. Chem.Phys 2012;405:124.
[25] Hoxha A, Locht R, Leyh B, Dehareng D, Hottmann K, Jochims HW, Baumgärtel H. Chem.Phys 2000;260:237.
[26] McLinden MO, Kazakov AF, Brown JS, Domanski PA. Int.J. Refrigeration 2014;38:80.
[27] Howard CJ. J. Chem. Phys. 1976;65:4771.
[28] Perry RA, Atkinson R, Pitts Jr JN. J. Chem. Phys. 1977;67:458.